Excited-state dynamics of the isolated ultracold ovalene molecule

A. Amirav, U. Even, and Joshua Jortner

Department of Chemistry, Tel-Aviv University, Tel Aviv, Israel
(Received 10 January 1980; accepted 13 March 1980)

In this paper we report the results of an experimental study of the energetics and the dynamics of the first two electronically excited singlet states S_1 and S_2 of the ovalene molecule ($C_{32}H_{14}$) seeded in supersonic beams of Ar and of Kr. By an optimal choice of the stagnation pressure (100–300 Torr) of the Ar and Kr carrier gases expanded through a 200 μ nozzle, efficient rotational–vibrational cooling of the large molecule was accomplished, while the spectrum was not obscured by the formation of van der Waals complexes. We have interrogated the energy-resolved fluorescence action spectrum, the time-resolved fluorescence, as well as the energy-resolved fluorescence of the bare, ultracold, isolated, large molecule. The first spin-allowed $^1S_0(^1A_{1g}) \rightarrow {}^1S_1(^1B_{3u}^-)$ transition with an origin at 21449 cm^{-1}, exhibits a sparse, well-resolved, vibrational level structure at low excess vibrational energies, E_V, while the higher energy range of S_1 reveals a congested level structure corresponding to overlapping resonances within a single electronic manifold. The time-resolved decay lifetimes of photoselected single vibronic levels of S_1 are in the range 1.7–2.2 μsec, exhibiting a very weak energy dependence on E_V and being close to the pure radiative lifetimes of S_1. The second $S_0(^1A_{1g}) \rightarrow S_2(^1B_{2u})$ transition of ovalene reveals an irregular, closely-spaced structure, resulting from strong interstate coupling between the S_2 and the S_1 electronic states, whose electronic origins are separated by ~ 1800 cm^{-1}. The strength function for the scrambling of the S_2 origin with the background S_1 manifold was extracted from the spectroscopic data, providing information on the energetics and on the energy dependence of interstate coupling. The time-resolved decay lifetimes of the scrambled S_2 molecular eigenstates are longer by about two orders of magnitude than the pure radiative lifetimes of S_2, as estimated from the integrated oscillator strength, manifesting the dynamic consequences of the intermediate level structure. The energy-resolved fluorescence resulting from excitation into the S_2 state exhibits emission in the $S_1 \rightarrow S_0$ energy region, which is in accord with the large dilution factor for the S_2–S_1 scrambling. The structure of the energy-resolved emission spectrum may provide some information regarding intrastate vibrational energy redistribution in this large molecule.

I. INTRODUCTION

The Born–Oppenheimer (BO) separability conditions usually provide an adequate starting point for the identification and the analysis of the energy levels of electronically excited states of polyatomic molecules. The implications of intramolecular nonadiabatic coupling between zero-order BO vibronic states, which correspond to different electronic configurations in "small" triatomic molecules are well understood,[1,2] being manifested by (a) spectroscopic implications, i.e., a rich absorption spectrum of mixed states[3]; and (b) lifetime effects, i.e., anomalously long radiative decay times of the lowest spin-allowed excited states of SO_2, NO_2, and CS_2.[4] These effects stem from the redistribution of the intensity of a zero-order doorway state, which carries oscillator strength from the ground state, among a large number of molecular eigenstates that are well separated in energy relative to their radiative widths, and which are active both in absorption and in emission. When two excited electronic states of a large molecule, e.g., the second S_2 singlet state and the first excited S_1 state are separated by a small gap, a low-lying vibronic level ϕ_s of S_2 will be effectively coupled to a sparse background manifold $\{\phi_k\}$ of S_1 vibronic levels. The low-lying levels of S_2 will be scrambled and, consequently, the absorption spectrum and the radiative decay characteristics of this second excited singlet state will exhibit the features of the small molecule limit encountered within a large molecule.[5] We shall refer to such characteristics of a large molecule as "intermediate strong coupling",[1] or rather as the "intermediate level structure",[6,7] in analogy to the terminology of nuclear physics.[8]

Experimental information regarding the small molecule characteristics of the energetics and of the decay features of the S_2 state of some large aromatic molecules, which exhibit intermediate level structure, stems from the following sources:

1. Spectroscopic information. The electronic origin of the second $S_2(^1B_{2u})$ singlet excited state of naphthalene is located at 3700 cm^{-1} above the electronic origin of the first $S_1(^1B_{3u}^-)$ excited singlet.[9,10] This molecule exhibits a characteristic intermediate level structure corresponding to the mixed molecular eigenstates in the absorption spectrum of S_2 in the low-temperature mixed crystal.[9–14]

2. Time-resolved studies in the low pressure vapor phase for the radiative decay of excited electronic–vibrational states in the vicinity of the S_2 configuration of 3,4-benzopyrene,[15,16] pyrene,[17] naphthalene,[18] chrysene,[19] and 3,4-benzophenantrene[19] reveal that in the low pressure gas phase the decay times considerably exceed the pure radiative lifetimes of the S_2 states. In all these molecules the S_2–S_1 electronic energy gap is relatively low (~ 3000–4000 cm^{-1}), and the peculiarities of the radiative decay exhibit the consequences of intramolecular S_2–S_1 level scrambling.[2,5,6,11–13]

The interpretation of the available spectroscopic and

 0021-9606/81/073745-12$01.00

lifetime data in terms of the modern theory of interstate coupling in large molecules takes some courage, as the theory considers interstate scrambling of a single vibronic level of an "isolated" molecule with the manifold of background state, focusing attention on the dynamic information resulting from photoselective excitation of a single molecular eigenstate or a well-defined wave packet of molecular eigenstates. The spectroscopic information concerning the intermediate level structure in the S_2 state of naphthalene was obtained in a mixed crystal,[9,10] as spectroscopic studies of large molecules in the low pressure gas phase at room temperature result in broad structureless and uninformative absorption bands. The broadening mechanisms of the absorption spectra of these "isolated" large molecules in the bulb result from thermal inhomogeneous broadening (TIB) effects, originating from rotational broadening as well as from vibrational sequence congestion. The TIB render an unambiguous spectroscopic identification and analysis of electronically–vibrationally excited states almost impossible. To overcome these effects of TIB on the absorption spectra, it was customary to conduct these studies on a guest molecule in a low-temperature mixed crystal[9,10] or in a Shpolskii matrix.[20] Unfortunately, such spectroscopic information, as that pertaining to the S_2 state of naphthalene, is complicated by "trivial" effects of inhomogeneous broadening due to the statistical distribution of trapping sites, as well as by "nontrivial" effects, originating from medium-induced vibrational relaxation within the S_1 background manifold, which results in line broadening of the molecular eigenstates.[21,22] Investigation of the time-resolved decay characteristics of these molecular eigenstates following short-time optical excitation of the "isolated" large molecules at room temperature[15–19] are hampered by TIB effects. Thermal population of rotational and vibrational levels in the ground state, together with the angular momentum selection rules for rotational excitation and the propensity rule $\Delta v = 0$ for the excitation of each of the nonsymmetric vibrational modes v results in a broad thermal distribution of excited rotational–vibrational levels of the molecule excited at room temperature by a "monochromatic" optical source. In fact, a genuine photoselective excitation of a large molecule cannot be accomplished at room temperature as the molecule carries its memory of the thermal population of the ground state to the electronically excited manifold. The severe effects of TIB on the absorption spectra and on the "preparation" of initially excited states of large molecules can be circumvented by the use of supersonic-free expansion in seeded molecular beams,[23,24] which result in ultracold, "isolated," large molecules, whose excited-state energetics[25–28] and decay dynamics[27,29–31] can be experimentally interrogated. We report the results of a study of the excited-state energetics and of the decay dynamics of the first two lowest excited singlet states S_1 and S_2 of the ovalene ($C_{32}H_{14}$) molecule seeded in supersonic molecular beams of Ar and of Kr. This molecule was explored by us as, on the basis of the currently available solution spectra of ovalene in 1-methylnaphthalene,[32,33] the S_2–S_1 energy gap is extremely low, being ~ 400 cm^{-1} in solution, whereupon the S_2 electronic state of this molecule is expected to correspond to the intermediate level structure, exhibiting the energetics and the decay characteristics of a heavily scrambled S_2–S_1 manifold. The combination of supersonic free expansion in seeded beams, together with energy-resolved and time-resolved spectroscopy, allows the increase of spectral resolution by three orders of magnitude over that achieved in bulb experiments or in thermal molecular beams, making possible the interrogation of the dynamics of truly photoselected vibrational states. The study of the S_2–S_1 mixing in the ovalene molecule presented herein demonstrates the nature and the significance of the information unveiled in the exploration of excited-state dynamics of ultracold, "isolated," large molecules.

II. EXPERIMENTAL DETAILS

Our supersonic beam apparatus uses a 6 in. diffusion pump (Varian VHS 6) backed by a rotating pump (Alcaltel) with a pumping speed of 500 l/min, which limits the stagnation pressure below 1000 Torr. Wharton, Smalley, and Levy[23,24] have introduced He as a carrier gas for laser spectroscopy in seeded supersonic beams and this practice was followed by several groups.[25,26,28,29,31] We have found that the degree of rotational and vibrational cooling of several molecules, e.g., iodine,[34] chromyl chloride,[34] tetracene,[27] pentacene,[34] and ovalene, seeded in supersonic jets of Ar and of Kr was much more efficient than in He. By an optimal choice of the pressure p of the Ar and Kr carrier gas in the range $p = 100$–300 Torr, which was expanded through a 200 μ nozzle, efficient rotational–vibrational cooling of large molecules, such as tetracene, pentacene, and ovalene, was accomplished, while the spectrum was not obscured by the formation of van der Waals complexes between the aromatic molecule and the rare-gas atoms. The supersonic expansion of ovalene (commercially supplied by Aldrich Chemicals) heated in the sample chamber to 325 °C (corresponding to a vapor pressure of 10^{-2} Torr[35] in Ar and Kr was conducted through a 200 μ nozzle, the backing pressure being 100–500 Torr. To eliminate the possibility of thermal decomposition of the ovalene sample to be catalyzed by our usual stainless steel sample holders and nozzles, the sample chamber and the nozzle were constructed from a ceramic material. Our interrogation method is based on monitoring fluorescence action spectrum, the time-resolved fluorescence and the energy-resolved fluorescence. A pulsed nitrogen-pumped dye laser (Molectron DL2) with a spectral width of 0.30 cm^{-1} and a temporal pulse width (HWHM) of 3 nsec crossed the supersonic beam at 7 mm down the nozzle. The total pressure in the excitation range was $\sim 10^{-2}$ Torr, so that the time between gas kinetic ovalene-Ar collisions is $\sim 10^{-5}$ s. Thus the ovalene molecule can be taken to be "isolated" on the relevant time scale (10^{-9}–10^{-6} s). The fluorescence was collected through a light pipe and detected by a photomultiplier (Hammamatsu R-936). The fluorescence excitation spectrum was recorded by a boxcar integrator after normalization to the laser intensity. Lifetimes were measured by a Biomation transient recorder (model 8100) and were averaged by a home-built signal averager. The energy-resolved fluorescence re-

sulting from laser excitation of the seeded jet at a fixed wavelength was collected and imaged by a lens onto the entrance slit of a monochromator and detected by a Phillips XP 1021 photomultiplier. The spectral resolution of the laser excited energy-resolved fluorescence spectrum was 7 Å.

III. SPECTROSCOPIC INFORMATION

A. Spectra of the bare molecule

Figure 1 shows the fluorescence excitation spectrum in the range 4700–4250 Å of ovalene seeded in Ar at the stagnation pressure of 210 Torr. No fluorescence could be detected by excitation at wavelengths above 4670 Å. We have demonstrated that the spectra of Fig. 1 originate from the "bare" ultracold molecule, rather than from van der Waals complexes, which can be formed between ovalene and the rare-gas atoms. The evidence rests on studies of the fluorescence excitation spectra of ovalene in Ar and Kr over the pressure range $p = 100$–800 Torr Ar and $p = 100$–400 Torr Kr. Figures 2 and 3 portray typical fluorescence excitation spectra of ovalene at several pressures of Ar and Kr. At $p > 200$ Torr of Ar and at $p > 100$ Torr of Kr the effects of hot vibrational bands and of vibrational sequence congestion are negligible. A careful examination of Figs. 2 and 3 reveals that, for Ar at $p = 350$ Torr and for Kr at $p = 270$ Torr, new weak spectral features appear on the low energy side of the main absorption bands. These new spectral features are assigned to ovalene–Ar and to ovalene–Kr complexes. The absorption bands attributed to van der Waals complexes are expected to increase quickly with increasing p, as for a sequential three-body collision mechanism for the formation of an ovalene–R_n (with R = Ar, Kr) complex, the corresponding absorption intensity is expected to increase as p^{2n}. This diagnostic criterion for the identification of van der Waals complexes is borne out by the spectral features which appear on the low energy side of the bare-molecule absorption bands, and which increase fast with increasing p. For Kr at 270 Torr the spectral features of the complexes are as intense as those of the bare molecule, while for Ar at $p = 740$ Torr the spectral features of the complexes dominate the spectra.

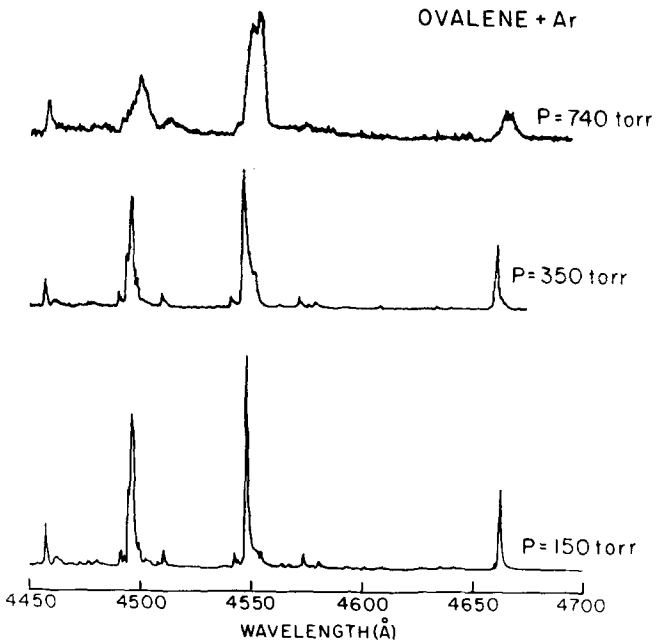

FIG. 2. Fluorescence excitation spectra of ovalene cooled in a supersonic expansion at several pressures of Ar. Backing pressures of Ar are indicated in the figure. All other experimental conditions as in Fig. 1.

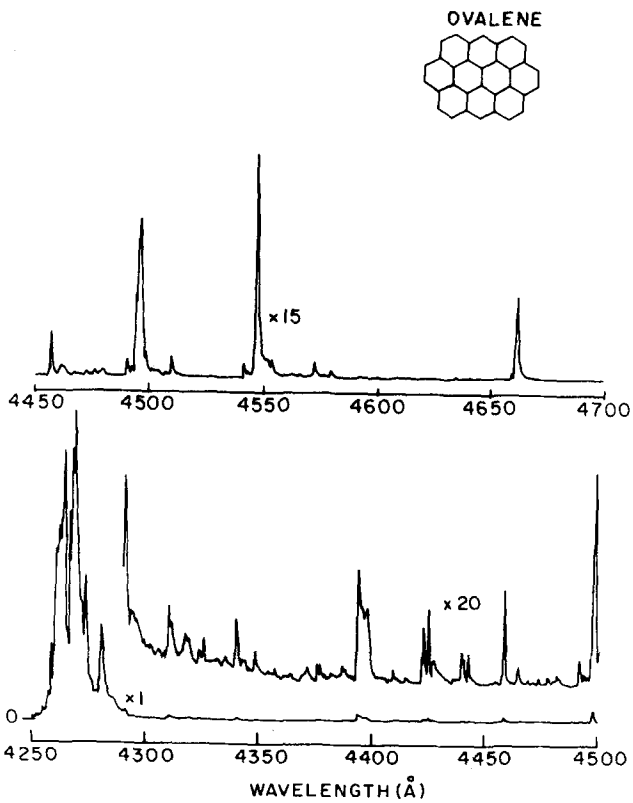

FIG. 1. Fluorescence excitation spectrum in the region 4700–4250 Å of ovalene cooled in a supersonic expansion. Ovalene (vapor pressure $\sim 10^{-2}$ Torr) was seeded into Ar at 210 Torr and was expanded through a 200 μ nozzle. The exciting dye laser has a bandwidth of 0.3 cm^{-1}. All fluorescence spectra are normalized to the laser intensity. The relative intensities are marked on the figure.

The excitation spectra of Fig. 1, which are attributed to the "bare" molecule, can be divided into two main energy regions.

(1) Region (1) spanning the energy range 4670–4300 Å. This energy region can be further subdivided into two ranges:

(1A) Range (1A) spanning the energy range 4670–4400 Å. This range exhibits well separated individual vibronic bands with individual spectral features having a width of ~4–5 cm^{-1}, presumably due to unresolved rotational structure.

(1B) Range (1B) covers the energy range 4400–4290 Å. In this range the spectrum of the ultracold molecule exhibits a congested spectrum revealing close-lying overlapping bands, which are superimposed on a background quasicontinuum.

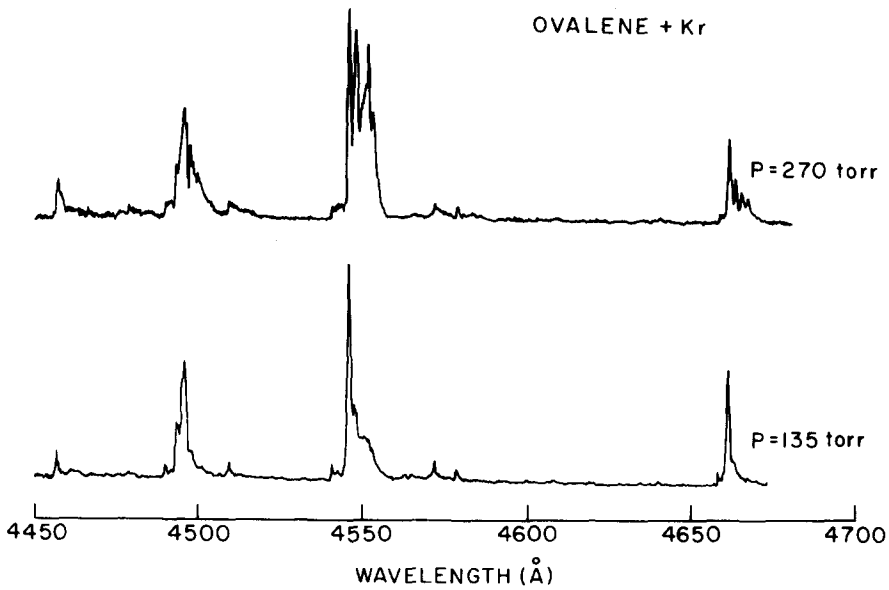

FIG. 3. Fluorescence excitation spectra of ovalene cooled in a supersonic expansion at several pressures of Kr. Backing pressures of Kr are marked on the figure. All other experimental conditions as in Fig. 1.

(2) Region (2) spanning the energy range 4300–4050 Å. The lowest wavelength of 4050 Å just reflects the highest energy where fluorescence excitation was conveniently detected with our experimental setup. The fluorescence excitation spectrum range (2) reveals an intense spectral transition, the peak intensities being 10–20 times higher than in region (1). The vibrational structure of the intense transition in the energy range 4300–4250 Å, which is magnified in Fig. 4, exhibits a large number of irregularly spaced spectral features with spacings of 5–20 cm^{-1} between peaks of consecutive bands.

On the basis of the vibrational structure and the drastically different intensities, we are compelled to assign regions (1) and (2) to two distinct electronic transitions of the bare, isolated, ultracold ovalene molecule, and we hsall now proceed to discuss these two distinct electronic excitations.

B. The $S_0 \rightarrow S_1$ transition

Region (1) is assigned to the lowest $^1S_0 \rightarrow {}^1S_1$ spin-allowed $\pi \rightarrow \pi^*$ transition of the ovalene molecule. Following the conventional classification of $\pi \rightarrow \pi^*$ electronic excitations of alternant aromatic hydrocarbons the lowest spin-allowed excited configuration of this molecule, which corresponds to the point symmetry group D_{2h}, can correspond either to the $^1B_{3u}^-$ state (^1L_b in Clar's notation)[32] or, alternatively, to the $^1B_{2u}$ (^1L_a) state. On the basis of the relative intensities of the three $\pi \rightarrow \pi^*$ electronic transitions of ovalene in solution,[32,33] the lowest excitation can be assigned to the $^1B_{3u}^-$ (^1L_b) state, whose allowed electric dipole component is polarized along the long molecular symmetry axis. The lowest-energy spectral feature of the ovalene molecule in the supersonic beam is located at 4662 Å (21 449 cm^{-1}). The absolute value of the wavelength scale is ± 2 Å (± 10 cm^{-1}), being determined by the accuracy of the calibration of the laser wavelength. This lowest-energy transition is tentatively assigned to the electronic origin of the lowest $S_0(^1A_{1g}) \rightarrow S_1(^1B_{3u}^-)$ transition of the ovalene molecule. It is still an open question whether the 21 449 cm^{-1} feature corresponds to the true 0–0 electronic origin or rather to a "false" vibronically induced origin. We favor the former alternative, which is supported by the analysis of the energy-resolved fluorescence spectrum reported in Sec. V.

It is instructive to compare the $S_0 \rightarrow S_1$ spectrum of the ultracold "isolated" molecule with the room temperature solution spectrum of this molecule.[32,33] The solution spectrum of the $S_0 \rightarrow S_1$ transition reveals a single broad (~ 100 cm^{-1}) absorption band peaking at 21 500 cm^{-1}. Two comments are now in order. First, the $S_0 \rightarrow S_1$ transition of ovalene exhibits only a modest red solvent shift in α-methylnaphthalene[32,33] relative to the electronic origin of the ultracold molecule. The magnitude of the solvent shift can only be qualitatively estimated as the solution spectrum is obscured by inhomogeneous broadening and by TIB effects. Second, and most important, the well-resolved $S_0 \rightarrow S_1$ spectrum of the ultracold large molecule provides a compelling demonstration for the potential of supersonic cooling for obtaining detailed spectroscopic information concerning the vibrational structure of electronic excited states of large molecules.

In Table I we present a preliminary vibrational analysis of the $S_0 \rightarrow S_1$ electronic transition of ovalene. Only the prominent absorption bands were listed. No attempt was made to analyze a large number of weak spectral features, some of which may be due to chemical and isotopic impurities. We have identified about eleven excited-state fundamental vibrations in the vibrational structure of the S_1 state, which are listed in Table I. Some of these excited-state fundamental vibrations of ovalene are exhibited also in similar but somewhat smaller aromatic hydrocarbons, such as 1,2-benzanthracene,[36] tetracene,[37,27] and perylene,[38] as is evident from Table II. The spectrum reveals some short vibrational progressions of the 544 cm^{-1} fundamental and of the 986 cm^{-1} fundamental, which consist of the $v = 0$, 1, and 2 members, indicating that configurational distortions between the S_1 excited state and the ground S_0 state

are relatively small. In view of the energetic proximity of the S_2 state (see Sec. III C), the relative intensities of the vibronic levels in the S_1 manifold may be affected by pseudo-Jahn–Teller coupling effects and further experimental work on the weak spectral features of this transition, combined with theoretical studies, is required for the elucidation of the vibronic structure of the S_1 manifold of ovalene.

It will be useful to consider a crude but useful classification of the vibrational structure of the $S_0 \rightarrow S_1$ transition, which were subdivided in Sec. III A into two ranges. Range (1a) is characterized by a sparse vibrational level structure, exhibiting well separated individual vibronic bands. In range (1a) the "preparation" of an individual vibrational state of S_1 by short-time optical excitation may be considered as meaningful and experimentally feasible. With the increase of excess vibrational energy the vibronic levels, which carry oscillator strength from the ground state, become more dense. The high-energy range of S_1, range (1b), exhibits a congested level structure, corresponding to overlapping resonances. In range (1b) not only fundamental frequencies and their combinations are optically active, but also effective anharmonic mixing between close-lying vibronic levels will enhance optical absorption to many other vibronic levels. This effect of intrastate vibrational mixing can be described as originating from many-levels Fermi resonances within a single electronic manifold. The appearance of the congested level structure in range (1b) within the S_1 electronic state of ovalene is analogous to the appearance of range (1b) in the $S_0 \rightarrow S_1$ transition of tetracene[27] and of pentacene.[34] We expect the appearance of such a congested vibrational level structure in the high energy region of the S_1 vibronic manifold of cold large molecules to constitute a general phenomenon. In region (1b) optical excitation of a single vibronic level cannot be accomplished. Rather, short-time excitation will result in a wave packet of nuclear vibrational states. The long-time optical excitation of such overlapping resonances observed in the absorption spectra provides the spectroscopic manifestation of intrastate intramolecular vibrational redistribution in large molecules.

TABLE I. A preliminary vibrational analysis of the S_1 state of the ovalene in a supersonic beam.

No.	λ[a] (Å)	ν[a] (cm^{-1})	$\Delta\nu$[b] (cm^{-1})	Assignment[c,d]
1	4662.2	21 449	0	0–0
2	4547.2	21 992	544	*F*
3	4496.2	22 241	793	*F*
4	4457.5	22 434	986	*F*
5	4443	22 507	1059	*F*
6	4440	22 522	1074	2×544 – 10
7	4425	22 599	1151	*F*
8	4422.5	22 612	1163	*F*
9	4398	22 738	1289	*F*
10	4393.5	22 761	1313	*F*
11	4348.5	22 996	1548	*F*
12	4340.5	23 039	1591	2×796 – 1
13	4325.9	23 117	1669	*F*
14	4317	23 164	1716	
15	4310.5	23 199	1751	986+793 – 28

[a]Accuracy of the absolute wavelength (λ) scale, determined by the accuracy of the calibration of the laser wavelength, is ±2 Å. The accuracy of the absolute frequency (ν) scale is ±10 cm^{-1}.

[b]$\Delta\nu$, excess vibrational energy relative to electronic origin. Accuracy ±5 cm^{-1}.

[c]*F*, fundamental.

[d]0–0, tentative assignment of electronic origin. This lowest energy band of the S_1 state can correspond to a false vibronically induced origin.

TABLE II. A comparison between the S_1 excited state fundamental frequencies of ovalene and the S_1 excited state frequencies of some other aromatic hydrocarbons: All frequencies in cm^{-1}.

Ovalene (Present work)	1,2 Benzanthracene[36]	Perylene[38]	Tetracene[27,37]
544	558	550	
793	793		
986	979		
1151			1151
1163			1166
1289	1259	1298	
1313	1343	1305	
1548			1549

C. The $S_0 \rightarrow S_2$ transition

Range (2) is assigned to the second $S_0 \rightarrow S_2$, spin-allowed, $\pi \rightarrow \pi^*$ transition. The S_2 state is attributed to excitation to the $^1B_{2u}$ electronic configuration, with the allowed transition dipole moment being polarized along the short molecular axis. The rather irregular closely-spaced structure of this electronic transition in the spectral range 4300–4250 Å (see Fig. 4) cannot be assigned to conventional vibrational structure, e.g., vibrational progressions. Rather, this structure is attributed to interstate nonadiabatic coupling between a single vibronic level of S_2 and a background manifold of vibronic levels which belong to the S_1 electronic configuration. The single vibronic level of S_2, which is effectively mixed and which is responsible for all the spectral features in the 4300–4250 Å spectral range, is assigned to the vibrationless electronic origin of S_2. As the intensity of the electronic origin of S_2 (zero order) state is considerably higher than that for each of the background S_1 (zero order) levels, the intensity due to transition to the mixed molecular eigenstates is high. The electronic energy gap between the S_2 and S_1 electronic states is $\Delta E \simeq 1800$ cm^{-1}, providing one of the lowest values of ΔE recorded for a large molecule. Now, the total density ρ_t of S_1 vibronic levels at the excess vibrational energy ΔE is moderately low, a very rough estimate being[39] $\rho_t \sim 10^4$–10^5 cm and the density ρ of the S_1 levels, which are effectively coupled to the electronic origin of S_2, constitutes only a fraction of ρ_t. Consequently, the

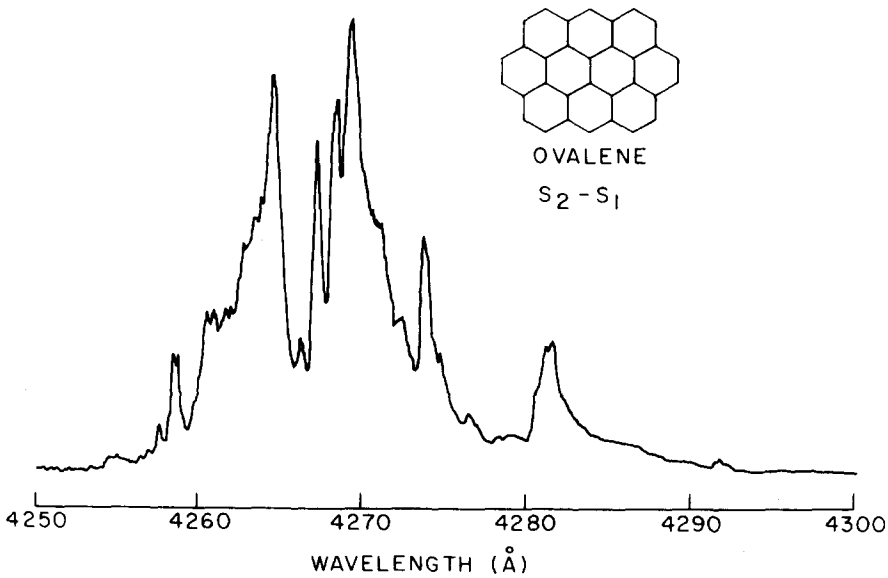

FIG. 4. Fluorescence excitation spectrum in the region 4300–4250 Å of ovalene cooled in a supersonic expansion of Ar. The backing pressure of Ar was 210-Torr and all other experimental conditions are identical to those in Fig. 1. The intensity scale is presented in arbitrary units.

mean spacing of the effectively coupled S_1 states is large relative to the widths $\langle\gamma_l\rangle$ of these levels which, according to the lifetime data of Sec. V, is $\langle\gamma_l\rangle \sim (2\ \mu s)^{-1} \sim 10^{-6}$ cm^{-1}. Thus, $\langle\gamma_l\rangle\rho \ll 1$ and the electronic origin of the S_2 (Fig. 4) state exhibits the characteristics of the intermediate level structure.[2,5-7] Up to date, spectroscopic evidence for the intermediate level structure has been recorded only for the S_2 state of naphthalene in a mixed crystal.[9,10] The present data provide detailed spectroscopic information regarding S_2–S_1 interstate scrambling, exhibiting the features of the intermediate level structure in an ultracold, "isolated," large molecule. Our experimental S_2 spectrum is only slightly smeared out by unresolved rotational structure, this inhomogeneous broadening effect amounting to ~4–5 cm^{-1}. Nevertheless, the spectroscopic data exhibit clearly and nicely the consequences of interstate scrambling between two closelying electronic states of a large isolated molecule.

A cursory comparison between the low-temperature spectrum of the isolated molecule and the room-temperature spectrum of ovalene in solution[32,33] is of some interest. The solution spectrum exhibits a typical low-resolution structure characteristic of high-temperature spectra of large aromatic hydrocarbons, revealing four broad bands with spacing of 1400 cm^{-1}, with the lowest band attributed to the inhomogeneously broadened and sequentially congested origin of the $S_0 \rightarrow S_2$ transition peaking at ~21 900 cm^{-1}. Two comments should be made at this point. Firstly, all the interesting spectroscopic features of interstate S_2–S_1 scrambling are obscured in the solution spectrum. Secondly, the solution spectral shift between the first peak of the S_2 band of the solution spectrum and the center of gravity of the scrambled electronic origin of S_2 in the ultracold, "isolated" molecule is 1500 cm^{-1} towards low energies. This red spectral shift reflects the effects of dispersive interactions on an intense electronic transition.[40] The spectral shift should be considered as a rough measure of environmental effects which cannot be analyzed in detail due to the limited information obtained from the smeared-out solution spectrum.

IV. THE STRENGTH FUNCTION FOR S_2–S_1 COUPLING

The interstate scrambling of the electronic origin of the S_2 state with its background S_1 manifold corresponds to the intermediate level structure. The optical absorption lineshape in range (2) (Fig. 4) is complicated, reflecting interstate coupling of a single $|s\rangle$ (S_2 origin) state with a background manifold of $\{|l\rangle\}$ (S_1) states, where the density of the $|l\rangle$ states is not sufficiently large to make coarse graining procedures applicable. Accordingly, the spectral distribution of the absorption strength cannot be characterized by a quasi-Lorentzian line shape, as is the case in the statistical limit, but rather the details of individual interstate coupling terms have to be taken into account. The interstate coupling can adequately be characterized by the weighted density of states,[2,6,7] or the strength function $\Gamma(E)$,

$$\Gamma(E) = \pi \sum_l |V_{sl}|^2 \delta(E - E_l)\ , \qquad \text{(IV.1)}$$

where V_{sl} is the nonadiabatic interstate coupling term, $\{E_l\}$ correspond to the energies of the zero-order E_l states, while E represents the photon energy. For the case of intermediate level structure $\Gamma(E)$ is energy dependent, in contrast to the statistical limit when $\Gamma(E)$ can be taken to vary only weakly with energy.

We shall now proceed to extract $\Gamma(E)$ from the experimental data in range (2). To do so it is convenient to adopt a representation of the $|l\rangle$ manifold which is prediagonalized in the total molecular Hamiltonian, so that we evade here the issue of intramolecular vibrational energy redistribution by using the nuclear eigenstates within each electronic configuration. In what follows we shall invoke one simplifying assumption, neglecting the (rather small) effects of rotational broadening, which can be taken into account by a proper convolution of our final result. The optical absorption lineshape $L(E)$ at the photon energy E is given (apart from irrelevant nu-

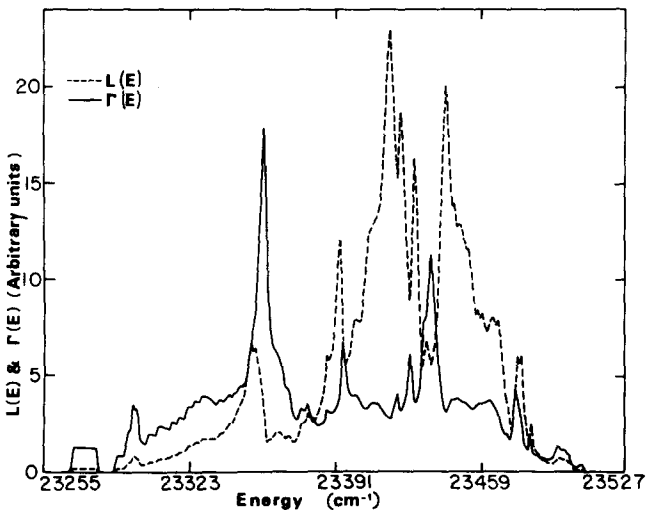

FIG. 5. The absorption spectrum $L(E)$ for the scrambled electronic origin $S_2(0)$ of the S_2 electronic state and the strength function $\Gamma(E)$ for the $S_2(0)-S_1$ coupling of ovalene, which corresponds to the intermediate level structure. The strength function was extracted from the experimental lineshape following the recipe outlined in Sec. V.

merical factors) in the form[6,7,11]

$$L(E) = -(E/\pi)|\mu_{gs}|^2 \mathrm{Im}G_{ss}(E) , \qquad \text{(IV.2)}$$

where μ_{gs} is the transition dipole moment from the ground state to $|s\rangle$, while Green's function is[6,7]

$$G_{ss}(E) = [E - E_s - \Delta(E) - i\Gamma(E)]^{-1} , \qquad \text{(IV.3)}$$

with $\Gamma(E)$ as the strength function, Eq. (IV.1), i.e., the imaginary part of the level shift, while the level shift $\Delta(E)$ can be expressed in terms of the dispersion relation

$$\Delta(E) = \frac{1}{\pi} PP \int \frac{\Gamma(E')dE'}{E - E'} , \qquad \text{(IV.4)}$$

with PP standing for the principal part of the integral. Equations (IV.1)–(IV.4) constitute a general expression for the line shape. The level shift and the strength function can be expressed in terms of the real and imaginary parts of Green's function[6,7,11–14]

$$\Gamma(E) = \frac{-\mathrm{Im}G_{ss}(E)}{[\mathrm{Re}G_{ss}(E)]^2 + [\mathrm{Im}G_{ss}(E)]^2} , \qquad \text{(IV.5a)}$$

$$E - E_s - \Delta(E) = \frac{\mathrm{Re}G_{ss}(E)}{[\mathrm{Re}G_{ss}(E)]^2 + [\mathrm{Im}G_{ss}(E)]^2} . \qquad \text{(IV.5b)}$$

The imaginary part of Green's function is obtained from the experimental spectrum using Eq. (IV.2), while the real part of $G_{ss}(E)$ is obtained by Berg's procedure[14] invoking the dispersion relation

$$\mathrm{Re}G_{ss}(E) = -\frac{1}{\pi} PP \int \frac{dE' \, \mathrm{Im}G_{ss}(E')}{E - E'} , \qquad \text{(IV.6)}$$

so that from the experimental line shape for the intermediate level structure, together with Eqs. (IV.2), (IV.6), and (IV.5), one can extract the strength function. This strength function for the S_2(origin)–S_1 coupling in ovalene is presented in Fig. 5, which yields two types of information:

(1) Spectroscopic information regarding the uncontaminated vibronic levels of the S_1 manifold in this energy range. This energetic information is quite useful.

(2) Information regarding the energy dependence of the interstate coupling emerges from the present analysis and is incorporated in the strength function.

It should be emphasized that the present analysis of the spectroscopic data starts from a $\{|l\rangle\}$, which is prediagonalized, whereupon a large number of $\{|l\rangle\}$ states, characterized by density of states $\rho \sim 10^3$–10^4 cm, is coupled to $|s\rangle$. The structure exhibited in the strength function can be interpreted in an alternative way, which is complementary to our analysis. One can envision a zero-order basis of vibronic $|\bar{l}\rangle$ states, consisting of normal modes and/or bond modes, so that anharmonic intrastate coupling now prevails between different $|\bar{l}\rangle$ states. The $|s\rangle$ doorway state is selectively coupled by intrastate nonadiabatic coupling to a (small) subset of $|\bar{l}\rangle$ states, which in turn are coupled via intrastate coupling to the rest of these $|\bar{l}\rangle$ levels. This alternative picture properly rationalizes the broadening of the bands in the optical spectrum, which can be assigned to intrastate vibrational redistribution. A quantitative analysis of the broadening is prohibited at present in view of inhomogeneous rotational broadening effects, which are still inherent in our spectrum. It should be emphasized that the strength function of Fig. 5 is independent of the choice of the basis set, and that in the analysis of the optical absorption line shape we have found it convenient to use a basis for which the $\{|l\rangle\}$ manifold is prediagonalized. The alternative segregation of the $|l\rangle$ manifold into two sets of levels, which are coupled among themselves by intrastate anharmonic coupling, just provides us with an alternative and perhaps more transparent description of the simultaneous effects of intrastate and interstate coupling in the vicinity of the origin of the S_2 state of ovalene.

V. TIME-RESOLVED EMISSION

A. General features

We have studied the time-resolved fluorescence decay of ovalene seeded in supersonic beams of Ar and of Kr, following photoselective excitation with a laser bandwidth of 0.3 cm^{-1}. Typical experimental time-resolved decay curves are presented in Fig. 6. The time-resolved fluorescence exhibited a single exponential decay mode over the time scale up to 3 μs. The decay lifetimes are summarized in Table III. It is apparent that the decay lifetimes both in region (1) and in region (2) are in the range 1.5–2.5 μs, being practically identical for the various vibronic components of $S_0 \rightarrow S_1$ transition, as well as for the scrambled electronic origin of the S_2 state. The relatively long (μs) experimental radiative decay times raise the distinct possibility that we were not monitoring a molecular decay rate but rather studying an "exodus effect" due to the electronically excited molecules leaving the interrogation region of the light pipe. To eliminate the possibility of such experimental artifact, we have compared the lifetimes of ovalene in Ar and in Kr. If the exodus effect is operative then the experimental lifetimes in these two gases are expected

to scale by the velocity ratio in these two beams, which is 1.4 in favor of Ar. The invariance of the experimental lifetime with respect to the nature of carrier gas (Table III) demonstrates that the time-resolved decay curves are unaffected by the "exodus effect" and the lifetimes are due to intrinsic excited state decay. In addition, the invariance of the lifetimes with respect to the nature and pressure of the carrier gas also indicates that the lifetimes are unaffected by collisions.

B. Time-resolved decay of the S_1 manifold

The fluorescence decay lifetimes[41] of the electronic origin of several vibronic components of the $S_0 - S_1$ transition exhibit a very weak dependence on the excess vibrational energy, the 20% variations of τ being only slightly outside the range of our experimental uncertainty. It is interesting to compare these experimental decay times with the pure radiative lifetime $\tau_r(S_1)$ of the S_1 state. A reasonable procedure for the estimate of $\tau_r(S_1)$ is based on the analysis of the integrated oscillator strength in solution according to the Strickler–Berg relation.[42] Unfortunately, this method could not be adopted for the S_1 state of ovalene in solution[32,33] because of the severe overlap of the $S_0 - S_2$ transitions. A rough estimate of the pure radiative lifetime $\tau_r(S_1)$ of S_1 was conducted by: (a) Evaluation of the ratio $I_{(S_0-S_1)}/I_{(S_0-S_{2(0)})}$ of the oscillator strength for the total $S_0 - S_1$ transition and the oscillator strength for the scrambled electronic origin of the $S_0 - S_2$ transition in the ultracold molecule. As the decay times are practically energy independent

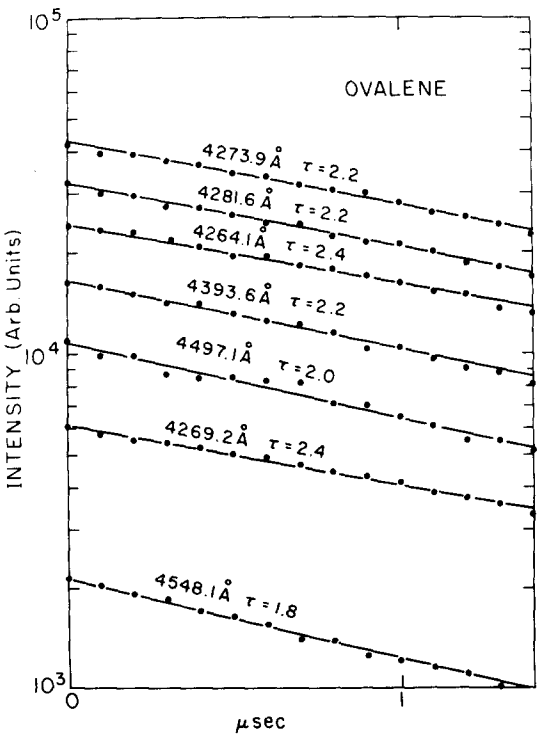

FIG. 6. Typical time-resolved radiative decay lifetimes for ovalene cooled in a supersonic expansion of 210 Torr Ar expanded through a 200 μ nozzle. The temporal pulse width (HWHM) of the dye laser was 3 ns. The excitation wavelengths (in Å) are marked on the lines. The lifetimes τ (in μs) are also indicated on the lines.

TABLE III. Fluorescence decay lifetimes of the ultracold isolated ovalene molecule.[a]

Excited state	λ (Å)	$\Delta\nu$[b] (cm^{-1})	τ[d] (μs)	Carrier gas
S_1	4662.2	0	2.0	Ar 210 Torr
	4547.2	544	1.8	Ar 210 Torr
	4547.2	544	1.7	Kr 270 Torr
	4552.5	VDWC[c]	1.7	Kr 270 Torr
	4496.2	793	2.0	Ar 210 Torr
	4393.5	1313	2.2	Ar 210 Torr
S_2 Scrambled	4281.5		2.2	Ar 210 Torr
	4273.9		2.2	Ar 210 Torr
	4269.5		2.4	Ar 210 Torr
	4264.7		2.4	Ar 210 Torr

[a]All lifetimes pertain to the bare molecule except for the 4552.5 Å band, which corresponds to ovalene–Kr van der Waals complex (VDWC).
[b]Frequency shift from origin of S_1.
[c]Ovalene–Kr VDWC.
[d]Accuracy of lifetimes τ, ±10%.

we have taken the ratio of the areas of all the spectral features in the excitation spectra for the $S_0 - S_1$ and for the intensity in region (2), respectively, which result in $I_{S_0-S_1}/I_{S_0-S_{2(0)}} \simeq 0.015$. (b) The relative intensity of the inhomogeneously and sequentially broadened 0–0 band in solution[33] corresponds to about $\eta = 0.25$ of the total intensity of the entire $S_0 - S_2$ transition. Thus, the ratio of the oscillator strengths for the $S_0 - S_1$ and $S_0 - S_2$ electronic transitions is

$$f_{(S_0-S_1)}/f_{(S_0-S_2)} = [I_{(S_0-S_1)}/I_{(S_0-S_{2(0)})}]\,\eta = 0.004 .$$

(c) The pure radiative lifetime of the $S_0 - S_2$ transition was estimated from the Strickler–Berg relation,[42] utilizing the solution data and resulting in $\tau_r(S_2) \sim 9$ ns. (d) The pure radiative lifetime for the $S_0 - S_1$ transition is

$$\tau_r(S_1) = [f_{(S_0-S_2)}/f_{(S_0-S_1)}]\tau_r(S_2) \simeq 2\ \mu s .$$

In view of the uncertainties the estimate $\tau_r(S_1) \simeq 2\ \mu$s should be considered to constitute just an order-of-magnitude estimate of the pure radiative lifetime of the S_1 state. The rough estimate of $\tau_r(S_1) \sim 2\ \mu$s is close to the experimental lifetimes of the individual vibronic levels of the S_1 state. Although the numerical agreement between the experimental values of τ and $\tau_r(S_1)$ should not be taken too seriously, it provides an indication that the major decay channel of individual vibronic levels in the S_1 manifold involves radiative decay.

Further support for the dominating role of the radiative channel in the decay of the S_1 states stems from two additional sources. First, the very weak energy dependence (or rather the independence) of the decay rate on the excess vibrational energy in range (1a) is distinct from the decay characteristic of range (1a) in the S_1 manifold of other large aromatic molecules, such as tetracene[27] and pentacene.[34] The decay characteristics of the S_1 state of ovalene are consistent with the interpretation that the two nonradiative $S_1 - T_1$ and $S_1 - S_0$ decay channels are rather ineffective. Second, we have failed to observe the enhancement of the nonradiative decay in the ovalene–Kr van der Waals complex. As is

evident from Table III the decay lifetimes of the bare ovalene and of the ovalene–Kr complex are identical. This insensitivity of the S_1 state of ovalene to a perturbation by a Kr atom is in contrast to the behavior of tetracene–Kr[30] and of pentacene–Kr[34] complexes, which reveal a marked enhancement of the $S_1 \sim T_1$ intersystem crossing induced by the external heavy atom effect. We conclude that the $S_1 \sim T_1$ intramolecular nonradiative channel is ineffective, presumably due to unfavorable vibrational overlap factors, so that heavy atom enhancement of the spin–orbit interstate electronic coupling is insufficient to enhance intersystem crossing. From the foregoing analysis we are led to the conclusion that the $S_1 \sim S_0$ and $S_1 \sim T_1$ nonradiative decay channels in the ovalene molecule are practically blocked in view of favorable Franck–Condon vibrational overlap factors. This conclusion is consistent with the analysis of the spectral features of the $S_0 \sim S_1$ transition (see Sec. III B), which indicate that nuclear configurational changes between the S_1 and the S_0 states are small in this very large molecule.

C. Time-resolved decay of the scrambled S_2 level

Experimental decay times were obtained following excitation in the spectral range 4260–4290 Å, which corresponds to the excitation of molecular eigenstates involving the scrambling of the electronic origin of S_2 among the S_1 manifold. The experimental lifetimes (Table III) in range (2) exhibit two notable features:

(a) These lifetimes $\tau \sim 2\ \mu$s are appreciably longer than the pure radiative lifetime $\tau_r(S_2) \simeq 9$ ns estimated on the basis of the integrated oscillator strength for the $S_0 \sim S_2$ transition in solution.[33] The ratio of the experimental and the pure radiative lifetimes is

$$\tau/\tau_r(S_2) \simeq 200\ . \tag{V.1}$$

(b) The values of τ in range (2) are very close to the decay times of the vibronic levels of the S_1 manifold.

The dramatic lengthening of the fluorescence decay times of the scrambled S_2 level [observation (a)] can adequately be interpreted in terms of the theory of intermediate level structure,[5–7] which envisions the decay of molecular eigenstates (ME's)

$$|m\rangle = \alpha_s^m |s\rangle + \sum_l \beta_l^m |l\rangle\ , \tag{V.2}$$

where $|s\rangle$ corresponds to the electronic origin of S_2, being characterized by the total decay width γ_s, while $\{|l\rangle\}$ represent the $\{S_1\}$ vibronic manifold with the decay widths γ_l. Provided that the ME's are well separated relative to their widths, independent excitation and decay of these ME's can be considered. This condition is well satisfied for the S_2–S_1 scrambling in ovalene as $\rho \sim 10^3$–10^4 cm for the effectively coupled levels and $\langle\gamma_l\rangle \sim 10^{-6}$ cm^{-1}, whereupon $\langle\gamma_l\rangle\rho < 1$. The experimentally observable reciprocal decay times γ_m of the ME's are

$$\gamma_m \simeq (\gamma_s/n) + \langle\gamma_l\rangle\ , \tag{V.3}$$

where $\langle\gamma_l\rangle$ is the mean decay width of the $\{|l\rangle\}$ manifold which, on the basis of our experimental lifetime data for S_1, is $\langle\gamma_l\rangle \simeq (2\ \mu\text{s})^{-1}$. n represents the dilution factor corresponding to the number of S_1 levels effectively coupled to the single S_2 level, which is given by[1,5]

$$n = 2\pi^2 V_{sl}^2 \rho^2\ , \tag{V.4}$$

where V_{sl} is the interstate S_2–S_1 nonadiabatic coupling, while ρ represents the density of effectively coupled levels in the S_1 manifold. As we are concerned here with the coupling of a single $|s\rangle$ state corresponding to the electronic origin of S_2 with the $\{S_1\}$ manifold, the dilution factor has to be expressed by Eq. (V.4) rather than in terms of the statistical expression of Deinun *et al.*[17] A crude estimate of the relevant energetic parameters can now be accomplished by using the approximate relation $\tilde{\Gamma}_s = 2\pi V_{sl}^2 \rho$ for the mean energetic spread of the energetic distribution of the ME's. From Fig. 4, $\tilde{\Gamma}_s \sim 100$ cm^{-1}, which, together with $\rho \sim 10^3$ cm, results in $V_{sl} \sim 1.2 \times 10^{-1}$ eV. The large value of V_l reflects the proximity of the S_2 and S_1 electronic states. From Eq. (IV.4) we now estimate $n \sim 3 \times 10^5$. The large value of the dilution factor is consistent with the experimental observation (b). As $\gamma_s/\langle\gamma_l\rangle = \tau_r(S_1)/\tau_r(S_2) \sim 200$, we expect that on the basis of Eq. (V.3) $\gamma_m = \langle\gamma_l\rangle(1 + \gamma_s/\langle\gamma_l\rangle n)$ $= \langle\gamma_l\rangle(1 + 200/n)$ with $n \sim 3 \times 10^5$, whereupon $\gamma_m \simeq \langle\gamma_l\rangle$ in accord with the experimental results. Thus, the dilution of the S_2 electronic origin among the molecular eigenstates is so effective that the decay lifetime of these molecular eigenstates is essentially determined by their S_1 character.

It is gratifying that the theoretical predictions regarding the small molecule decay characteristics of an electronically excited state of a large molecule, which corresponds to the intermediate level structure, are exhibited in a large ultracold ovalene molecule.

VI. ENERGY-RESOLVED EMISSION FROM THE SCRAMBLED S_2 LEVEL

The large dilution factor $n \sim 3 \times 10^5$ for the mixing of the electronic origin of S_2 with the background S_1 manifold is expected to lead to an interesting energy-resolved fluorescence spectrum originating from excitation into range (2) of the isolated ovalene molecule. According to Nitzan *et al.*[5] two spectral regions in the emission spectrum, resulting from excitation into the molecular eigenstates (V.2), can be distinguished; the high-energy s emission region[5] where S_2 fluorescence is exhibited and the low-energy l emission region[5] where the S_1 emission occurs. The time and energy integrated relative yield in the s region with respect to the yield in the region is

$$\gamma_s/\gamma_l \simeq \Gamma_s^{(r)}/n\langle\Gamma_l^{(r)}\rangle\ , \tag{VI.1}$$

where $\Gamma_s^{(r)}$ and $\langle\Gamma_l^{(r)}\rangle$ represent the pure radiative widths of S_2 and S_1, respectively. Utilizing Eq. (V.1), we take $\Gamma_s^{(r)}/\langle\Gamma_l^{(r)}\rangle = \tau/\tau_r(S_2) = 200$ which, together with $n \sim 3 \times 10^5$, results in the ratio $\gamma_s/\gamma_l \sim 10^{-3}$, whereupon the s fluorescence yield is expected to be negligible.

This prediction is borne out by the experimental study of the energy-resolved emission spectrum of ovalene excited into range 2. In Fig. 7 we present the low resolution (spectral resolution $\delta_r = 7$ Å) emission spectrum of ovalene in a supersonic nozzle excited at 4271 Å. For

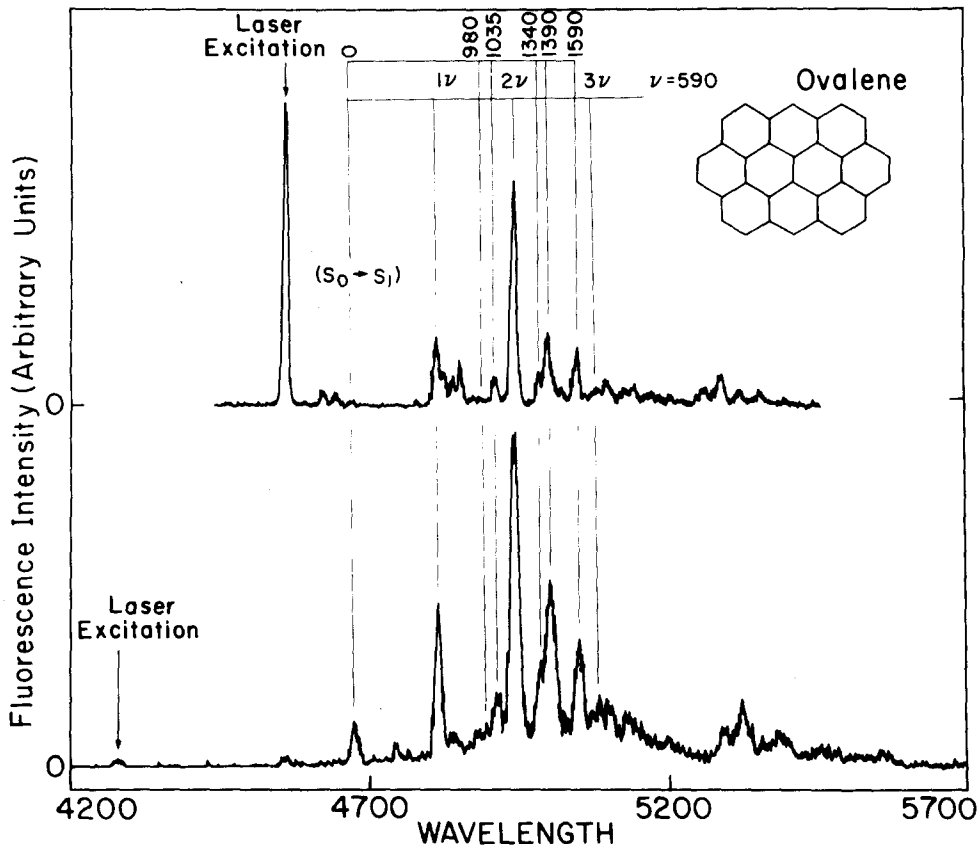

FIG. 7. Energy-resolved fluorescence spectra of ovalene cooled in a supersonic expansion (210 Torr Ar expanded through a 200 μ nozzle) and excited at 4271 Å (lower curve) and at 4547 Å (upper curve). The positions of the laser excitations are marked by arrows. The origin of the 0–0 band for $S_0 \rightarrow S_1$ in absorption is marked by an arrow. The maxima of the peaks in the fluorescence spectrum, resulting from excitation at 4271 Å, are marked by their energy spacings (in cm^{-1}) from the origin band.

the sake of comparison, we have also displayed in the upper part of Fig. 7 the emission spectrum of this molecule excited at 4547 Å, which corresponds to the 544 cm^{-1} vibration of the $S_0 \rightarrow S_1$ transition (range 1). The emission spectrum following excitation at 4271 Å in range 2 exhibits the following features:

(1) The emission in the range 4271–4650 Å is negligibly small.

(2) The emission is exhibited in the range 4650–5500 Å.

(3) The emission consists of peaks superimposed on a broad background.

(4) The emission peaks resulting from excitation in range 2 are considerably broader (FWHM $\simeq$ 70 cm^{-1}) than the linewidth of the emission, due to excitation in range 1 (FWHM = 32–40 cm^{-1}). The latter widths originate from instrumental broadening, being close to the claimed spectral resolution of 7 Å. We conclude that the broadening of emission peaks, resulting from excitation in range 2, is intrinsic.

(5) The lowest emission peak is located at 4664 Å which, within the experimental uncertainty of the spectral resolution (±5 Å), coincides with the 0–0 transition of the $S_0 \rightarrow S_1$ excitation of this molecule.

(6) The emission peaks (see Fig. 6) reveal a vibrational progression of 590 ± 20 cm^{-1}, as well as additional frequencies of 980, 1035, 1340, 1390, and 1590 cm^{-1}, all of which can be determined within an accuracy of ±20 cm^{-1}.

The emission spectrum of the ovalene excited into range 2 originates from excitation of ME's, resulting from the scrambling of $S_2(0-0)$ with the S_1 manifold, which are located about 1800 cm^{-1} above the electronic origin of the S_1 configuration. We shall now proceed to comment on the specific implications of these dynamic features of the emission following excitation in range 2:

(a) No emission in the s region is observed.

(b) The observable emission (4700–5500 Å) is due to the l region.

(c) The lack of observable of the resonance-type s fluorescence from the scrambled excited state of this large isolated molecule is in accord with the prediction $\gamma_s/\gamma_l \sim 10^{-3}$ based on Eq. (VI. 1).

(d) In this isolated huge molecule, $S_2 \rightarrow \{S_1\}$ intramolecular relaxation does not occur for the intermediate level structure. The lack of observable s fluorescence originates from a dilution effect on the character of the electronic origin of S_2, which is spread among $n \sim 3 \times 10^5$ ME's.

(e) The structure of the emission spectrum of the ultracold molecule in the l range reflects several peaks superimposed on a broad background. Even the distinct peaks are quite broad, the upper limit for their widths being ~ 70 cm^{-1}. The broadening of the main peaks, as well as the broad background in the emission spectrum of the ultracold molecule, originates from the existence of a fairly dense density of molecular eigenstates $\rho \sim 10^3 - 10^4$ cm. Our laser excitation by a spectral band-

width of ~0.3 cm^{-1} results in a bunch of ~10^2–10^3 excited ME's, which are now active in emission. The l character of these excited ME's involves different vibrationally excited states of S_1 located at ~1800 cm^{-1} above the S_1 origin. As the vibrational frequencies in the ground S_0 electronic configuration and in the S_1 electronically excited state are different, the emission from the bunch of the excited ME's will be appreciably broadened.[26] Excitation within the total spectral width of ~0.3 cm^{-1} (or even a lower coherent width) will result in an emission with a width of ≤ 70 cm^{-1}. The emission spectrum reflects the memory of the initial distribution of the vibrational states of the vibrationally excited S_1 manifold, which contributes to the initially excited ME's. The width ~70 cm^{-1} of these emission bands cannot be solely attributed to the effect of vibrational relaxation, but does reflect the dynamic consequences of the intrastate vibrational energy redistribution in the vibrationally electronically excited states of a large molecule.

Finally, we shall briefly comment on the spectroscopic information stemming from the emission in the l range, bearing in mind that these bands are intrinsically broadened, each being due to the decay of a bunch of excited ME's. This intrinsic broadening bears some resemblance to thermal vibrational sequence congestion except that the intrinsic vibrational broadening is homogeneous (except for some rotational broadening effects exhibited in our spectra), while the vibrational sequence congestion involves an inhomogeneous broadening effect. The peak of the lowest band in the emission spectrum coincides, within the experimental uncertainty, with the position of the electronic origin of the $S_0 - S_1$ transition. This observation provides strong support for our assumption that the electronic origin of the $S_0 - S_1$ transition involves the genuine electronic origin, corresponding to the 0–0 excitation, as proposed in Sec. III B. The vibrational progression of 590 ± 20 cm^{-1} observed in the emission spectrum is assigned to a ground state vibration whose excited state counterpart is the 544 cm^{-1} vibration (see Table I). The observation of this progression indicates that the 544 cm^{-1} spectral feature in absorption (Fig. 1 and Table I) involves a fundamental totally symmetric vibration. Finally, we note that the ground state vibrations (980 ± 20), (1035 ± 20), and (1590 ± 20) cm^{-1} have their counterparts in the excited state vibrational frequencies 986, 1059, and 1548 cm^{-1}.

VII. CONCLUDING REMARKS

We have explored the intramolecular dynamics of molecular eigenstates resulting from strong interstate coupling between two close-lying electronic configurations of a large molecule. The studies of energy-resolved excitation, combined with probing time-resolved and energy-resolved decay, demonstrate the potential of the use of laser spectroscopy in seeded supersonic beams to interrogate the intramolecular dynamics in "isolated," "bare," ultracold, large molecules, where the effects of medium perturbations and of vibrational (but not rotational) TIB were eliminated. The detailed study of the intermediate level structure of the S_2 electronic origin of ovalene is of considerable interest, as it exposes the spectroscopic and the dynamic implications of intrastate and interstate coupling, as well as the distinction between the consequences of intramolecular interstate coupling and intramolecular interstate electronic relaxation. As for the scrambled S_2 origin of ovalene $\tilde{\Gamma}_s \sim 100$ cm^{-1}, a coherent excitation of this zero-order $S_2(v=0)$ state is not feasible with the currently available light sources. Even with subpicosecond pulses only a bunch of ME's can be excited and these will exhibit the dynamic characteristics of the intermediate level structure which were explored by us.

ACKNOWLEDGMENT

This research was supported in part by the United States–Israel Binational Science Foundation (Grant 1404), Jerusalem, Israel.

[1] M. Bixon and J. Jortner, J. Chem. Phys. **50**, 3284 (1969).
[2] J. Jortner, J. Chim. Phys. **67**, 9 (1970).
[3] R. E. Smalley, L. Wharton, and D. H. Levy, J. Chem. Phys. **63**, 4977 (1974).
[4] A. E. Douglass, J. Chem. Phys. **45**, 1007 (1966).
[5] A. Nitzan, J. Jortner, and P. M. Rentzepis, Proc. R. Soc. London, Ser. A **327**, 367 (1972).
[6] S. Mukamel and J. Jortner, in *The World of Quantum Chemistry*, edited by R. Daudel and B. Pullman (Reidel, Boston, 1974), p. 145.
[7] S. Mukamel and J. Jortner, in *Molecular Energy Transfer*, edited by R. D. Levine and J. Jortner (Wiley, New York, 1975), p. 178.
[8] *Intermediate Level Structure in Nuclear Reactions*, edited by H. P. Kennedy and R. Schrils (University of Kentucky, Lexington, Kentucky, 1968).
[9] D. S. McClure and O. Schnepp, J. Chem. Phys. **23**, 1575 (1955).
[10] J. Wessel, Ph.D. thesis, University of Chicago, 1971).
[11] J. Jortner, S. A. Rice and R. M. Hochstrasser, in *Advances in Photochemistry*, edited by B. O. Pitts and G. Hammond (Wiley, New York, 1969).
[12] C. A. Langhoff and G. W. Robinson, Chem. Phys. **6**, 34 (1974).
[13] G. W. Robinson and C. A. Langhoff, Chem. Phys. **5**, 1 (1974).
[14] J. O. Berg, Chem. Phys. Lett. **41**, 547 (1976).
[15] P. A. Geldof, R. P. H. Rettschnick, and G. J. Hoytink, Chem. Phys. Lett. **4**, 59 (1969).
[16] P. Wannier, J. Jortner, and P. M. Rentzepis, Chem. Phys. Lett. **10**, 102 (1971).
[17] T. Deinun, C. J. Werkhoven, J. Langelaar, R. P. H. Rettschnick, and J. D. W. van Voorst, Chem. Phys. Lett. **27**, 210 (1974).
[18] P. Wannier, J. Jortner, and P. M. Rentzepis, Chem. Phys. Lett. **10**, 193 (1971).
[19] J. Langelaar, M. W. Leeuv, J. D. W. van Voorst, and R. P. H. Rettschnick, Chem. Phys. Lett. **62**, 14 (1979).
[20] E. V. Shpolskii, Soviet Phys. Usp. **5**, 522 (1962); **6**, 411 (1963).
[21] T. J. Aartsma and D. A. Wiersma, Phys. Rev. Lett. **36**, 1360 (1976).
[22] T. E. Orlowski and A. H. Zewail, J. Chem. Phys. **70**, 1390 (1979).
[23] D. H. Levy, L. Wharton, and R. E. Smalley, in *Chemical and Biochemical Applications of Laser* (Academic, New York, 1977), Vol. 2, p. 1.
[24] D. H. Levy, L. Wharton, and R. E. Smalley, Acc. Chem. Res. **10**, 134 (1977).
[25] P. S. H. Fitch, L. Wharton, and D. H. Levy, J. Chem. Phys. **69**, 3424 (1978).

[26]P. S. H. Fitch, L. Wharton, and D. H. Levy, J. Chem. Phys. **70**, 2019 (1979).
[27]A. Amirav, U. Even, and J. Jortner, J. Chem. Phys. **71**, 2319 (1979).
[28]B. Soep and A. Tramer, Chem. Phys. Lett. **64**, 465 (1979).
[29]F. M. Behlen, M. Mikami, and S. A. Rice, Chem. Phys. Lett. **60**, 364 (1979).
[30]A. Amirav, U. Even, and J. Jortner, Chem. Phys. Lett. **67**, 9 (1979).
[31]R. Campargue and B. Soep, Chem. Phys. Lett. **64**, 469 (1979).
[32]J. B. Birks, in *Photophysics of Aromatic Molecules* (Wiley-Interscience, London, 1970), p. 75.
[33]*U. V. Atlas of Organic Compounds* (Butterworth, London, 1968).
[34]A. Amirav, U. Even, and J. Jortner (to be published).
[35]H. Inokuchi and H. Akamatu, in *Solid State Physics*, edited by F. Seitz and D. Turnbull (Academic Press, New York, 1961), Vol. 12, p. 93.
[36]N. A. Fenina, Opt. and Spectrosc. (USSR) **11**, 428 (1966).
[37]N. J. Kruse and G. J. Small, J. Chem. Phys. **56**, 2985 (1972).
[38]R. I. Personov, E. I. Alshitz, L. A. Bykovskaya, and B. M. Kharlamov, Sov. Phys. JETP **38**, 912 (1974).
[39]The very rough estimate for the total densities of ρ_t of S_1 states of ovalene for the excess vibrational energy of $E_V = 1800\ \mathrm{cm}^{-1}$ was obtained by taking the calculated value[17] for the density of states of pyrene $\rho \sim 5\times 10^2$ cm at this E_V and scaling $\rho_t = [\rho]^{S_1/S_2}$ where $S_1 = 132$ and $S_2 = 78$, representing the numbers of vibrational degrees of freedom in ovalene and in pyrene, respectively.
[40]H. C. Longuett-Higgins and J. A. Pople, J. Chem. Phys. **27**, 192 (1957).
[41]We believe that the μs lifetimes recorded by us cannot be assigned to hot phosphorescence for the first triplet state of ovalene. It may be argued that $S_1 \rightarrow T_1$ internal conversion is sufficient resulting in population of T_1. We exclude such a possibility as the μs decay lifetimes are too short to be assigned to radiative decay (characterized by reasonably high phosphorescence quantum yield) of a triplet state of an alternate aromatic hydrocarbon. Further evidence against efficient $S_1 \rightarrow T_1$ intersystem crossing in ovalene is based on the lack of heavy atom effect on the radiative decay, which is discussed in Sec. II B.
[42]S. J. Strickler and R. A. Berg, J. Chem. Phys. **37**, 814 (1962).